

The Microbiologically Influenced Corrosion of L245NS Carbon Steel by Sulfate-Reducing Bacteria in H₂S Solutions

Haobo Yu^{1,*}, Lei Ma^{1,2}, Zimo Li¹, Ruijing Jiang¹

¹ Department of Materials Science and Engineering and Beijing Key Laboratory of Failure, Corrosion and Protection of Oil/Gas Facilities, China University of Petroleum (Beijing), Changping District, Fuxue Road 18, Beijing 102249, P. R. China

² Research Institute of Oil and Gas Engineering, PetroChina Tarim Oilfield Company, Korla 841000, P. R. China

*E-mail: Yu_h_b@sina.com

Received: 5 June 2018 / Accepted: 23 July 2018 / Published: 1 September 2018

The influence of sulfate-reducing bacteria (SRB) on the corrosion of L245NS carbon steel was investigated in a medium containing H₂S by various surface characterizations and electrochemical measurements. The addition of H₂S will totally inhibit the planktonic SRB in the medium. However, the sessile SRB in the corrosion crust can survive under the protection of the biofilm. Pitting corrosion is found under the corrosion crust, which is caused by the sessile SRB. The pitting corrosion rate is 1.1 mm/a. Additionally, the corrosion rate increases with the corrosion time. The SRB influenced corrosion mechanism of the steel is discussed.

Keywords: Carbon steel, Sulfate-reducing bacteria, Hydrogen sulfide, Microbiological corrosion, Pitting corrosion

1. INTRODUCTION

Corrosion has become one of the primary issues that result in pipeline failures and induce disasters, which causes enormous economic losses in oil and gas fields[1–3]. Microorganisms are present in various environments, such as subterranean water, soil, sea water, and oilfield produced water. The life activities of microorganism can cause severe metal corrosion, called microbiologically influenced corrosion (MIC)[4–7]. It has been reported that more than 20% of pipeline corrosion failures are related to MIC[8]. Among various types of microorganisms, anaerobic sulfate-reducing bacteria (SRB) are the most commonly encountered corrosive microbes in MIC pitting against

pipelines and facilities in oilfields[8–10]. In the natural environment, SRB normally exist in a community called biofilm[11–13]. A biofilm consists of extracellular polymeric substances (EPS), biocorrosion products, and embedded sessile cells[14]. In SRB MIC, the biofilm could shuttle electrons from the extracellular iron oxidation across the cell wall into the cytoplasm where the sulfate is reduced[13,15]. SRB attack the iron via withdrawal of electrons, so this first type of MIC can be called EMIC (electrical microbially influenced corrosion)[16]. On the other hand, SRB damage iron constructions indirectly through a corrosive chemical agent formed by the organisms as the dissimilatory product from the sulfate reduction with organic compounds or hydrogen, such as H₂S and organic acids[17,18]. Because the biofilm can block acid diffusion, the local pH under the biofilm would be much lower than the pH of the solution, and consequently, a local corrosion is induced[19]. This type of MIC is called CMIC (chemical microbially influenced corrosion)[16]. For both MIC types, the biofilm plays an important role in the corrosion caused by SRB.

In an acidic oilfield, the produced water often contains H₂S, which threatens pipeline integrity and operator safety[20–22]. It was found that H₂S has a direct and reversible toxic effect on SRB and will inhibit SRB growth[23,24]. When the H₂S concentration is higher than 547 mg/L, the SRB growth will be completely inhibited in solution[23]. However, in reality, the SRB can attach to the steel surface and then form a biofilm. The biofilm may separate the sessile cells from the solution with a high concentration of H₂S[19]. Thus, the SRB may still survive and multiply underneath the biofilm, thus causing MIC. To date, few studies on SRB corrosion in H₂S solutions have been reported.

In this study, the corrosion of the L245NS pipeline steel under SRB biofilms in H₂S solutions was investigated. Electrochemical measurements, including potentiodynamic polarization and electrochemical impedance spectroscopy (EIS), and materials analysis techniques, i.e., scanning electron microscopy (SEM), energy-dispersive X-ray spectrum (EDS), and laser scanning confocal microscopy (LSCM), were used to study the corrosion behaviour. The mechanistic aspects of the steel corrosion in the corrosive environments containing both dissolved H₂S and SRB were also discussed.

2. MATERIALS AND METHODS

2.1 Material and specimens

The test specimens were cut from an L245NS pipeline steel. The chemical composition is shown in Table 1. The size of specimens for immersion tests was 50 mm × 10 mm × 3 mm. The specimens for electrochemical tests were machined to a disc with a thickness of 8 mm and a diameter of 12 mm. All the specimens were ground by using 400, 600, 800 and 1200 grit silicon carbide papers. In particular, the electrode surface was polished by using a diamond paste with a grain size of 1.5 μm. Prior to use, every specimen was rinsed with distilled water and ethyl alcohol and then sanitized using an ultraviolet (UV) lamp for 30 min.

Table 1. Chemical composition of L245NS (in wt%)

C	Si	Mn	P	S	Cr	Mo	Ni	Nb	Ti	Fe
0.11	0.21	0.86	0.01	0.003	0.056	0.026	0.026	0.002	0.001	Bal.

2.2 SRB cultivation

The SRB seed used in this study was obtained from the produced water of an oilfield in northwestern China. The SRB culture medium was Postgare's C medium, which contained 6.0 g sodium lactate, 4.5 g Na₂SO₄, 1.0 g NH₄Cl, 1.0 g yeast extract, 0.5 g KH₂PO₄, 0.3 g sodium citrate, 0.06 g CaCl₂·6H₂O, 0.06 g MgSO₄·7H₂O and FeSO₄·7H₂O and 1 L deionized water. The pH of this solution was adjusted to 7.2 ± 0.1 by using 0.1 M NaOH and 0.1 M HCl solutions. The culture media were autoclaved at 121°C for 20 min and then cooled down to room temperature. Then, the SRB culture was obtained after 1 day of incubation.

2.3 Immersion test

The immersion tests were conducted at 38°C for 7 days. Before the test, the solution was deaerated using a high-purity N₂ stream for 1 h and allowed to stand for 2 h for SRB to attach to the metal surface. Then, H₂S gas was bubbled into the solution until the end of the test. After the test, the surface films formed on steel specimens were removed by using a pickling solution containing an imidazoline derivative inhibitor. The exposed surfaces of the specimens were rinsed with distilled water, cleaned in ethyl alcohol, and dried in a high-purity N₂ stream. Uniform corrosion rate of the specimen was calculated by:

$$R_{corr} = \frac{(w_1 - w_2) \times 8.76}{\rho A t} \times 10^3 \quad (1)$$

where R_{corr} is the uniform corrosion rate, mm/y; w_1 is the specimen initial weight, g; w_2 is the weight of the specimen after removing the corrosion product, g; A is the area of the specimen, cm²; t is the corrosion time, hour; and ρ is the density of the metal, g/cm³.

2.4 Electrochemical test

All electrochemical measurements were performed by using an electrochemical workstation (Reference 600, Gamry) in a three-electrode cell, where the steel specimen, a platinum sheet and a saturated calomel electrode (SCE) were used as the working electrode, the counter electrode and the reference electrode, respectively. Electrochemical impedance spectroscopy (EIS) was measured at a stable open circuit potential (OCP) with a 10-mV sinusoidal voltage signal within the frequency range of 10⁻² to 10⁵ Hz. ZSimpWin software was used to analyse the EIS data. Potentiodynamic polarization curves were recorded by sweeping the potential from -1.1 V_{SCE} to 0.1 V_{SCE} at a scan rate of 2 mV/s.

2.5. Surface analysis

The structure and the composition of corrosion films formed on the immersion test specimen were examined by using an FEI Quanta 200F scanning electron microscope (SEM). Before the SEM test, the specimen, which was soaked in the SRB culture, was fixed in a 5% glutaraldehyde solution for 3 h and washed with phosphate buffered saline (PBS) and distilled water. Then, the specimen was immersed in a gradient series of ethanol (50%, 75%, and 99%) solutions for dehydration. The pitting corrosion was analysed by laser scanning confocal microscopy (OLS4100, Olympus) after removing the corrosion film.

3. RESULTS

3.1 Corrosion rate

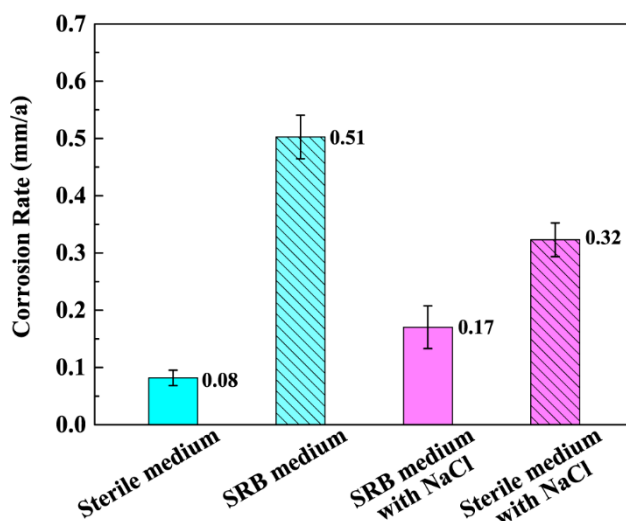


Figure 1. The uniform corrosion rates of L245NS in Postgate's C media bubbled with H₂S gas at 38°C after a 7-day immersion test. The concentration of NaCl is 10 g/L.

Fig. 1 shows the uniform corrosion rates of L245NS after a 7-day immersion test in the sterile and SRB Postgate's C media bubbled with H₂S gas at 38°C. Compared to the sterile medium, the corrosion rate in the medium with SRB increased from 0.08 mm/a to 0.51 mm/a. For comparison, the Postgate's C medium with NaCl (10 g/L) was also studied. Similarly, in Postgate's C medium with NaCl, the corrosion rate also increased from 0.17 mm/a to 0.32 mm/a after the addition of SRB. Combining the corrosion rates in different media, the results show that, in both saturated H₂S media with and without NaCl, the corrosion rates of the specimens are accelerated significantly by SRB, which means that the SRB can maintain the metabolic activity in the saturated H₂S environment and promote the corrosion rate of L245NS specimens.

In the sterile medium, the only factor causing corrosion is the H_2S gas that was bubbled into the solution. Because of the addition of NaCl, the concentration of Cl^- increased in the medium, which can accelerate the H_2S corrosion rate by expediting the anodic reaction and destroying the corrosion product layer[25,26]. The corrosion rate increased after NaCl was added to the sterile medium, as shown in Fig. 1. However, in the SRB culture, SRB is another corrosion factor besides H_2S . Although Cl^- can accelerate the corrosion caused by H_2S , at the same time, NaCl addition will increase the osmotic pressure of the medium and then inhibit the growth of the bacteria[27]. Hence, the MIC caused by SRB will be deaccelerated by NaCl. This is the reason that the corrosion rate of L245NS decreased from 0.51 mm/a to 0.32 mm/a after adding NaCl in the SRB culture (Fig. 1).

3.2 Distribution of SRB

After the 7-day immersion test in Postgate's C medium bubbled with H_2S gas, the SRB in the corrosion solution and the corrosion product formed on the specimen surface were checked separately by the MPN method according to ASTM D4412. To eliminate the effect of the H_2S dissolved in the corrosion solution and absorbed on the corrosion product, both were purged with N_2 for 2 hours. Then, the corrosion solution and the corrosion product were put in SRB test bottles. The test bottles were kept at $38^\circ C$ for 7 days. The colour of all the test bottles did not change in the first hour, suggesting that the H_2S dissolved in the corrosion solution and absorbed on the corrosion product were removed completely and did not affect the SRB test results.

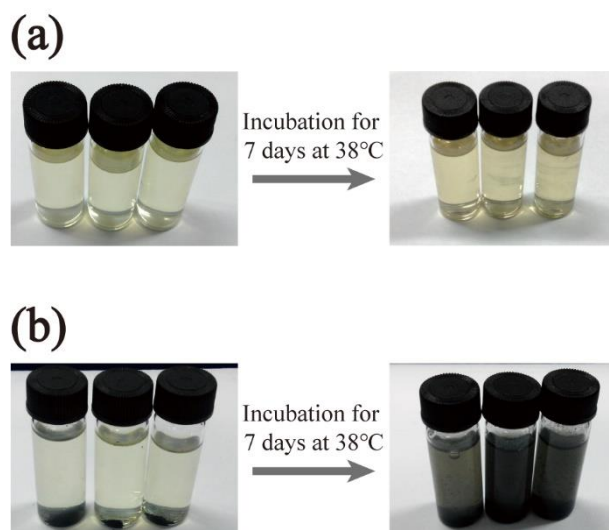


Figure 2. The test of SRB in corrosion solutions (a) and corrosion products (b) after experiments

After the 7-day bacterial culture, the colour of SRB test bottles for corrosion solutions did not change, as shown in Fig. 2. This means that the planktonic SRB cannot live in the saturated H_2S aqueous solution, which is consistent with Reis's result[23]. However, in contrast, the colour of the SRB test bottles for corrosion products changed from yellow to opaque black. The result indicates that the sessile SRB can only survive in the corrosion product and induce the SRB corrosion.

3.3 Corrosion morphology and product analyses

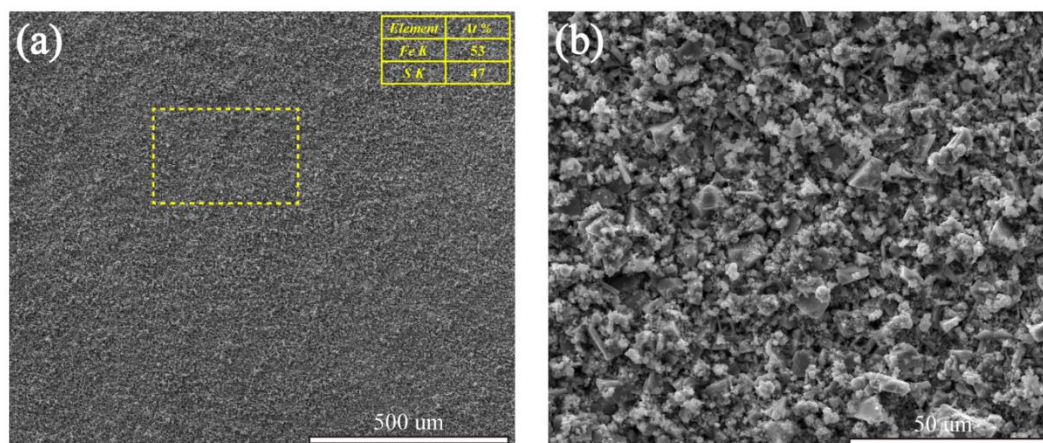


Figure 3. SEM morphology of specimens after the 7-day immersion test in the sterile Postgate’s C medium bubbled with H₂S gas at 38°C. The table at the top right corner in Fig. 3(a) is the EDS result of the elemental composition of corrosion products in the region marked by a yellow frame.

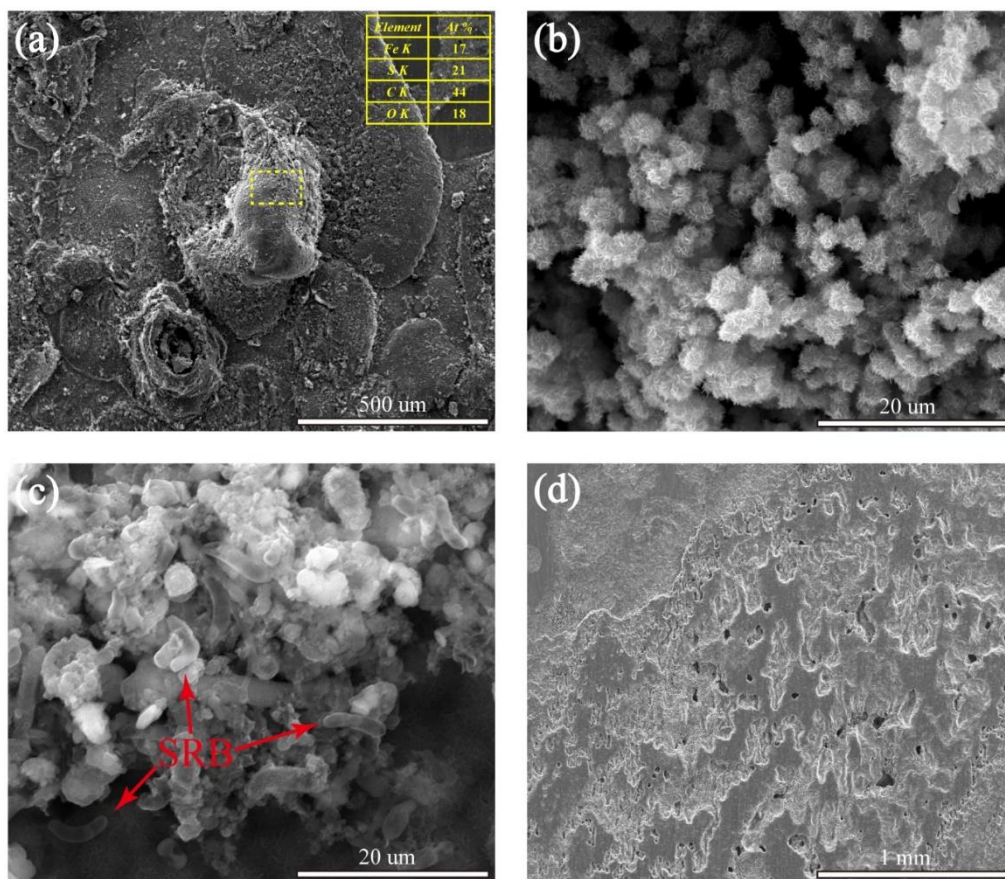


Figure 4. SEM morphology of specimens after the 7-day immersion test in the SRB Postgate’s C medium bubbled with H₂S gas at 38°C. (a) Corrosion crust and EDS result of the elemental composition of the region marked by a yellow frame; (b) surface of the corrosion crust; (c)

SRB under the corrosion crust; (d) surface morphology of specimens after removal of the surface film.

Fig. 3 shows the micromorphology of the specimen surface after the 7-day immersion test in the sterile Postgate's C medium bubbled with H_2S gas at $38^\circ C$. As exhibited in Fig. 3, in the sterile medium, the corrosion product is flat, uniform and compact, and formed by tiny crystals. EDS analysis shows that these corrosion products contain 53% Fe and 47% S elements. There is no apparent pitting corrosion seen on the specimen surface.

Fig. 4 shows the micromorphology of the specimen surface after the 7-day immersion test in the SRB Postgate's C medium bubbled with H_2S gas. In the presence of SRB, the morphology of the surface is different from that of the pure H_2S corrosion. As shown in Fig. 4(a), there are numerous corrosion crusts formed on the specimen surface. The composition of the corrosion crust was obtained by EDS, and the result shows that the corrosion crust contains not only Fe and S but also C and O (Fig. 4(a)). Fe and S come from ferric sulfide, which is the product of both the H_2S corrosion and the SRB metabolite. C and O only come from the biofilm generated by SRB. Hence, the corrosion crust is composed of ferric sulfide and the biofilm.

Fig. 4(b) is the SEM image of the surface of the corrosion crust. The image shows that there is no SRB on the crust surface. However, by removing the top of the corrosion crust, abundant SRB cells were found under the corrosion crust, and all the SRB are long and rod-shaped, as seen in Fig. 4(c). This is because the outside surface of the corrosion crust was immersed in the saturated H_2S solution. The dissolved H_2S with a high concentration has a direct toxic effect on the SRB. Hence, the SRB cannot live on the surface of the corrosion crust. However, the biofilm can protect the SRB from the harmful external environment[19], so the SRB can grow and reproduce under the corrosion crust. The SEM morphology results are consistent with the distribution of SRB in section 3.2. After removing the corrosion crust, the pitting corrosion was found on the specimen surface, as shown in Fig. 4(d). The depth of corrosion pitting was analysed by LSCM. The maximum pitting depth after the 7-day corrosion in the SRB solution reaches $20.9\ \mu m$ (Fig. 5). The pitting corrosion rate is $1.1\ mm/a$, which is much higher than the uniform corrosion rate.

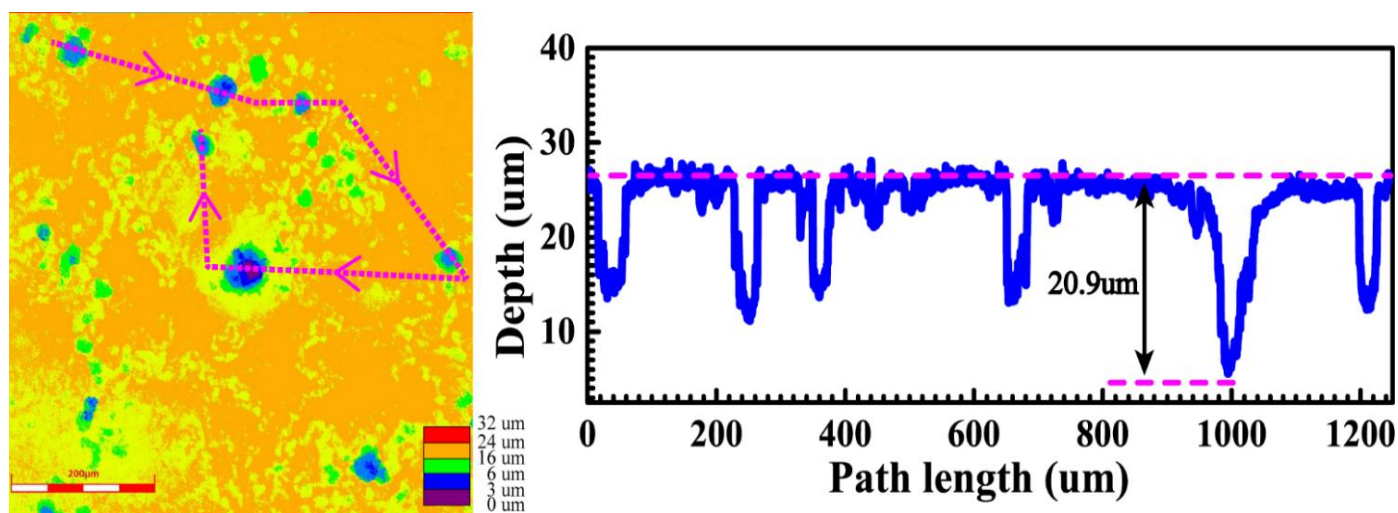


Figure 5. 3-D images of the deepest pits for the L245NS specimen immersed in the SRB medium obtained by laser scanning confocal microscopy.

3.4 Electrochemical measurements

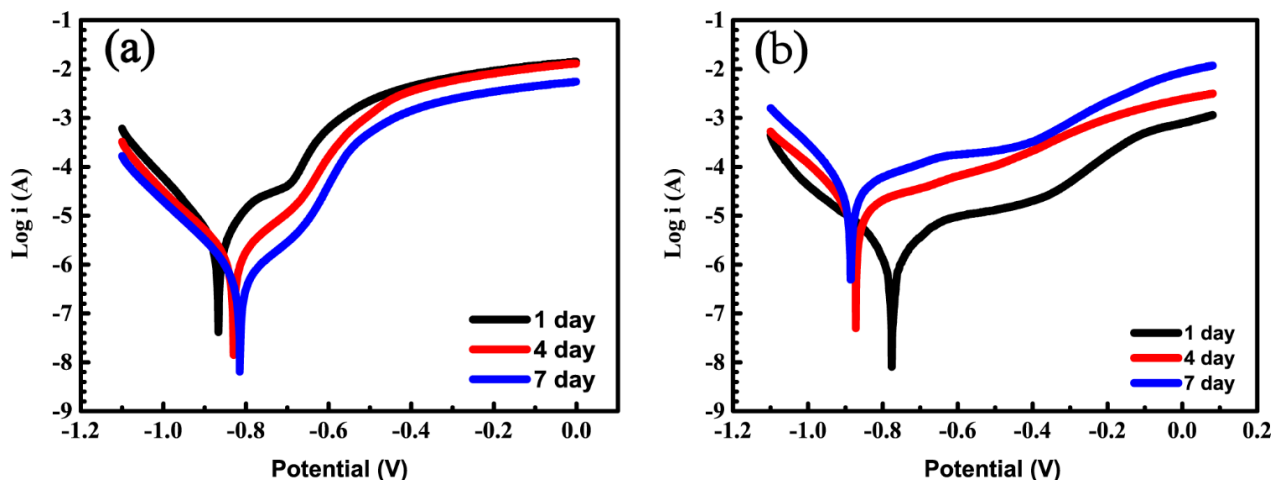


Figure 6. Potentiodynamic polarization curves of the specimens after the 1-day, 4-day and 7-day immersion tests in the sterile (a) and SRB (b) Postgate’s C media bubbled with H₂S gas at 38°C.

Fig. 6 shows the potentiodynamic polarization curves of the specimens after the 1-day, 4-day and 7-day immersion tests in the sterile and SRB Postgate’s C media bubbled with H₂S gas at 38°C. The fitted polarization parameters are shown in Table 3. For the sterile solution, with increasing time, E_{corr} (corrosion potentials) increased, i_{corr} (corrosion current density) decreased and β_a (anodic Tafel slope) increased, which suggests that the corrosion is reduced. However, for the SRB solution, E_{corr} decreased, and i_{corr} and β_b (cathodic Tafel slope) increased, which means that the MIC increased over time. Additionally, it can be clearly observed that the cathode current density increased with time.

The EIS data were measured in both sterile and SRB Postgate’s C media on the first, the fourth, and the seventh day during the 7-day immersion test. The Nyquist plots are shown in Fig. 7. In the sterile solution, the Nyquist plot diameter increases with the corrosion time. However, in the SRB solution, the Nyquist plot diameter decreases with the corrosion time. The results suggest that with an increase in the corrosion time, the protection of corrosion products formed in the sterile H₂S solution is increased. Nevertheless, in the SRB solution, increasing corrosion time led to more severe corrosion.

Table 3. Potentiodynamic polarization parameters of specimens after the 1-day, 4-day and 7-day immersion tests

Duration (day)	E_{corr} (V vs. SCE)	i_{corr} (uA/cm ²)	β_a (mV/dec)	β_b (mV/dec)
Abiotic medium				
1	-0.86	4.12	417	-855
4	-0.83	1.72	745	-874

7	-0.80	0.61	849	-824
SRB medium				
1	-0.78	2.92	275	-794
4	-0.86	17.18	261.	-635
7	-0.88	50.71	248	-577

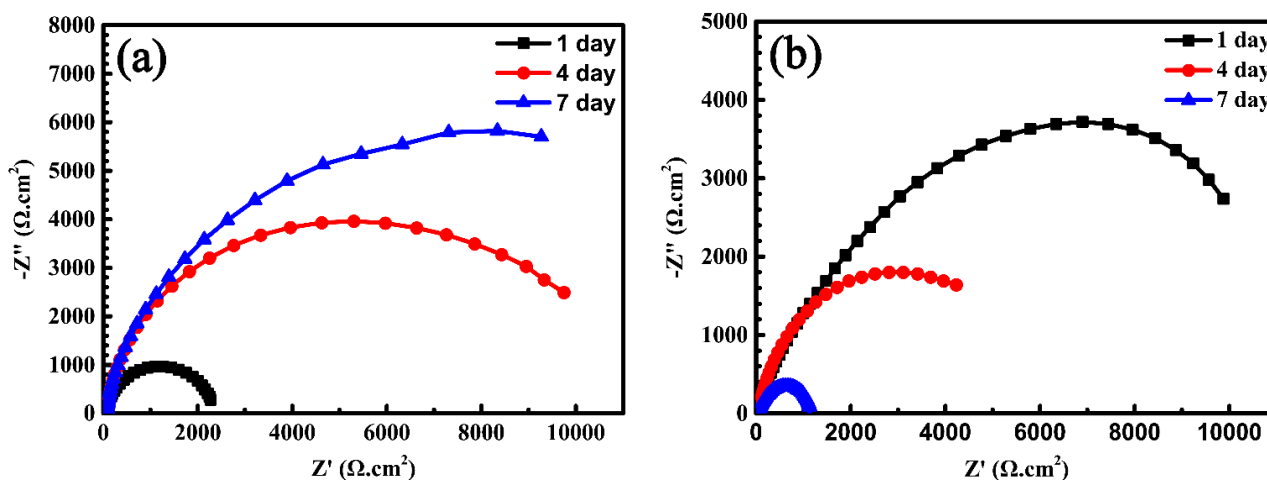


Figure 7. Nyquist plots of the specimens during the 7-day immersion test in the sterile (a) and SRB (b) Postgate's C media bubbled with H₂S gas at 38°C.

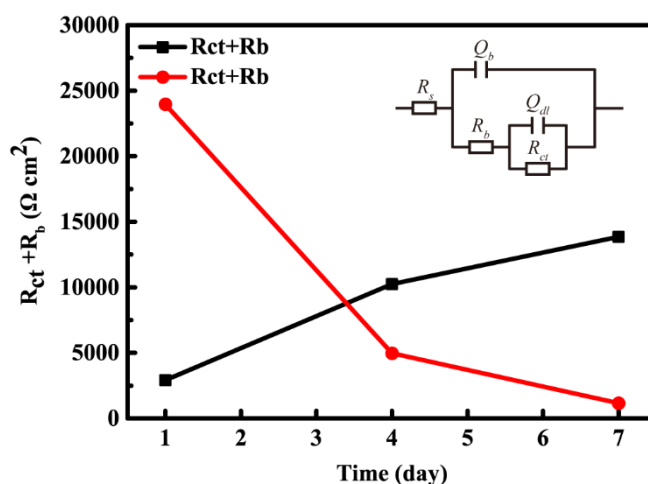


Figure 8. Equivalent circuits and time courses of $R_{ct}+R_b$ during the 7-day immersion test in the sterile and SRB Postgate's C media bubbled with H₂S gas at 38°C. R_s : the solution resistance; R_b : the resistance of the biofilm or the corrosion product film; R_{ct} : the charge transfer resistance; Q_b : the capacitance of the biofilm or the corrosion product film; Q_{dl} : the double layer capacitance.

The impedance spectra of specimens immersed in the sterile and SRB Postgate's C media were analysed by using an equivalent electrical circuit. The impedance spectra were fitted with a two-time constant circuit model. The circuit model is shown in Fig. 8. In the equivalent electrical circuit, R_s , R_b and R_{ct} stand for the solution resistance, the resistance of the biofilm or the corrosion product film, and the charge transfer resistance, respectively. Q_b and Q_{dl} stand for the capacitance of the biofilm or the

corrosion product film and the double layer capacitance, respectively. The impedance of constant phase element (CPE) was employed, which is expressed as follows:

$$Z_Q = Y_0^{-1} (j\omega)^{-n} \quad (2)$$

where Y_0 and n are CPE parameters and ω is the angular frequency (rad/s). The quantitative fitting results are shown in Table 4 and Fig. 8. $R_{cr}+R_b$ is closely related to the corrosion rate, and a higher value means a lower corrosion rate and vice versa[28]. $R_{cr}+R_b$ values for sterile specimens increase significantly with the immersion time, suggesting a decrease in the charge transfer between the metal surface and the corrosion product film, which means a decreased corrosion rate. In contrast, $R_{cr}+R_b$ values for SRB specimens decrease with the immersion time, which implies that the charge transfer between the metal surface and the biofilm becomes faster, and the MIC is increased.

Table 4. EIS parameters of specimens during the 7-day immersion test

Duration (day)	R_s ($\Omega \text{ cm}^2$)	Y_b ($\Omega^{-1} \text{ cm}^{-2} \text{ s}^n$)	n_b	R_b ($\Omega \text{ cm}^2$)	Y_{dl} ($\Omega^{-1} \text{ cm}^{-2} \text{ s}^n$)	n_{dl}	R_{ct} ($\Omega \text{ cm}^2$)
Abiotic medium							
1	0.1	0.004	0.8	64.54	0.00002	0.98	2843
4	0.6	0.002	0.9	65.58	0.00023	0.88	10180
7	0.6	0.042	0.8	66.62	0.00035	0.98	13790
SRB medium							
1	3.1	0.022	0.9	67.23	0.0001	0.95	23880
4	4.3	0.017	0.8	40.85	0.0024	0.84	4931
7	4.4	0.012	0.9	40.21	0.00038	0.72	1128

4. DISCUSSION

It is commonly accepted that a high concentration of H_2S has toxic effects on SRB[24]. Reis suggested that a hydrogen sulfide concentration of 547 mg/L (16.1 mM) will completely inhibit SRB growth[23]. In this study, H_2S was bubbled into the Postgate's C medium continuously. The solution is a saturated H_2S solution. Based on the H_2S equilibrium at 38°C reported by Ning.[29], the corresponding H_2S concentration in the liquid reaches 2.6 g/L, which significantly exceeds the tolerance range of SRB. However, the immersion test suggests that the corrosion rates of specimens in the sterile and SRB solutions are 0.08 mm/a and 0.51 mm/a, respectively. The corrosion rate in the SRB solution is much higher than that in the sterile solution (Fig. 1), indicating that the SRB can still survive and promote corrosion in the saturated H_2S solution. After the immersion test, the distribution of SRB was analysed. The results indicate that only the sessile SRB can survive under the corrosion crust, and the planktonic SRB will be totally inhibited in the solution, as shown in Fig. 2 and Fig. 4. This is because the corrosion crust consists of the corrosion product and the biofilm. The biofilm can control the migration of organic and inorganic compounds between the internal and the external parts of the biofilm[17,18,30,31]. H_2S cannot enter the biofilm, so the sessile SRB can grow and propagate under the corrosion crust, as shown in Fig. 2 and Fig. 4.

It is widely accepted that anaerobic MIC, such as MIC caused by SRB, can be categorized into two main types based on microbial metabolisms, namely, respiration and fermentation[32]. In MIC involving SRB respiration, an external non-oxygen oxidant, such as sulfur, serves as the terminal electron acceptor. Organic carbons are used as electron donors during the normal growth. The electron transport chain provides energy to SRB in anaerobic respiration. In a saturated H₂S solution, the SRB can only live under the biofilm. Because the biofilm will hinder the mass transfer from the solution to the inside of the biofilm, the access to organic carbons through the biofilm may have also been limited. Therefore, SRB, which is under the biofilm, may change the electron donor from the carbon source to the element Fe. SRB extracts energy from iron to couple its oxidation with sulfate reduction for survival. At the same time, the Fe substrate is corroded. MIC involving SRB fermentation is caused by the secreted corrosive metabolites, such as organic acids produced by organic carbon oxidation. Due to organic acid production, the pH around SRB cells can be very low. However, in this study, the biofilm will hinder the transfer of organic carbons to SRB; hence, this work mainly addresses MIC involving respiration.

In the sterile H₂S solution, the corrosion product, iron sulfide, will form and cover the specimen surface and thus affect the corrosion process. At the beginning, the corrosion product is thin, loose and not uniform, so the protection performance is weak. However, with increasing time, the corrosion product becomes compact and complete, which can protect the substrate well. Hence, $R_{ct}+R_b$ increased from 2907 $\Omega\text{ cm}^2$ to 13856 $\Omega\text{ cm}^2$, i_{corr} decreased from 4.12 $\mu\text{A/cm}^2$ to 0.61 $\mu\text{A/cm}^2$, and also the β_a increased, as shown in Fig. 6(a), Fig. 7(b) and Table 3. In a biotic solution, the corrosion process is controlled by SRB. When SRB cells attach to a metal surface, they will generate biofilms with EPS, which can cover and protect the sessile SRB cells and the substrate surface. At the initial stage, the low bacterial number and the biofilm protection of the substrate against H₂S cause a slight corrosion. With increasing time, the sessile SRB propagate under the biofilm, which would induce the decrease of $R_{ct}+R_b$ from 23947 $\Omega\text{ cm}^2$ to 1168 $\Omega\text{ cm}^2$, the increase of i_{corr} from 2.92 $\mu\text{A/cm}^2$ to 50.71 $\mu\text{A/cm}^2$ and β_b from -794 mV/dec to -577 mV/dec. The MIC induced by increasing SRB respiration is aggravated, as seen in Fig. 5~Fig. 7. Therefore, under the protection of the biofilm, the sessile SRB can survive and reproduce in the H₂S solution, causing a serious pitting corrosion.

5. CONCLUSIONS

In this paper, the microbiologically influenced corrosion of L245NS carbon steel by sulfate-reducing bacteria in H₂S solutions was investigated. It was discovered that the planktonic SRB will be totally inhibited in Postgate's C medium bubbled with H₂S gas. Only the sessile SRB can survive under the protection of the biofilm formed on the metal surface. In the SRB medium, the corrosion rate was 0.51mm/a, which was higher than in pure H₂S solution. And also, a serious pitting corrosion caused by the sessile SRB occurred. The pitting corrosion rate reached 1.1 mm/a. With corrosion time, the $R_{ct}+R_b$ decreased from 23947 $\Omega\text{ cm}^2$ to 1168 $\Omega\text{ cm}^2$, and the i_{corr} increased from 2.92 $\mu\text{A/cm}^2$ to 50.71 $\mu\text{A/cm}^2$, which was different from pure H₂S corrosion and indicated that the corrosion was controlled by the SRB.

References

- Lekan popoola, *Springer*, 4 (2013) 35.
2. X. Lei, H. Wang, F. Mao, J. Zhang, M. Zhao, A. Fu, Y. Feng and D. D. Macdonald, *Corros. Sci.*, 131 (2018) 164.
 3. S. Nešić, *Corros. Sci.*, 49 (2007) 4308.
 4. D. Xu, R. Jia, Y. Li and T. Gu, *World J. Microbiol. Biotechnol.*, 33 (2017) 97.
 5. H. Liu, D. Xu, A. Q. Dao, G. Zhang, Y. Lv and H. Liu, *Corros. Sci.*, 101 (2015) 84.
 6. R. Jia, D. Yang, D. Xu and T. Gu, *Sci. Rep.*, 7 (2017) 1.
 7. F. Batmanghelich, L. Li and Y. Seo, *Corros. Sci.*, 121 (2017) 94.
 8. R. Jia, D. Yang, I. K. Salleh, J. M. M. Ibrahim, H. B. A. Rahman, P. A. Hamid and T. Gu, *Corrosion*, 125 (2017) 1.
 9. J. Xu, C. Sun, M. Yan and F. Wang, *Int. J. Electrochem. Sci.*, 7 (2012) 11281.
 10. H. Liu, D. Xu, K. Yang, H. Liu and Y. F. Cheng, *Corros. Sci.*, 132 (2018) 46.
 11. A. R. Padmavathi, M. Periyasamy and S. K. Pandian, *Bioresour. Technol.*, 188 (2015) 185.
 12. L. T. Dall'Agnol, C. M. Cordas and J. J. G. Moura, *Bioelectrochemistry*, 97 (2014) 43.
 13. P. S. Stewart and M. J. Franklin, *Nat. Rev. Microbiol.*, 6 (2008) 199.
 14. Y. Li, D. Xu, C. Chen, X. Li, R. Jia and D. Zhang, *J. Mater. Sci. Technol.*, 34 (2018) 1713.
 15. R. Jia, D. Yang, J. Xu, D. Xu and T. Gu, *Corros. Sci.*, 127 (2017) 1.
 16. D. Enning and J. Garrelfs, *Appl. Environ. Microbiol.*, 80 (2014) 1226.
 17. I. A. C. Pereira, A. R. Ramos, F. Grein, M. C. Marques, S. M. da Silva and S. S. Venceslau, *Front. Microbiol.*, 2 (2011) 1.
 18. M. Magot, G. Ravot, X. Campaignolle, B. Ollivier, B. K. Patel, M. L. Fardeau, P. Thomas, J. L. Crolet and J. L. Garcia, *Int. J. Syst. Bacteriol.*, 47 (1997) 818.
 19. T. Gu, *J. Microb. Biochem. Technol.*, 04 (2012) 3.
 20. M. A. Lucio-garcia, J. G. Gonzalez-rodriguez, M. Casales, L. Martinez and J. G. Chacon-nava, *Corros. Sci.*, 51 (2009) 2380.
 21. W. Zhao, Y. Zou, K. Matsuda and Z. Zou, *Corros. Sci.*, 102 (2016) 455.
 22. L. Zhang, X. Tang, Z. Wang, T. Li, Z. Zhang and M. Lu, *Int. J. Electrochem. Sci.*, 12 (2017) 8806.
 23. M. a Reis, J. S. Almeida, P. C. Lemos and M. J. Carrondo, *Biotechnol. Bioeng.*, 40 (1992) 593.
 24. R. Jia, J. L. Tan, P. Jin, D. J. Blackwood, D. Xu and T. Gu, *Corros. Sci.*, 130 (2018) 1.
 25. Q. Y. Liu, L. J. Mao and S. W. Zhou, *Corros. Sci.*, 84 (2014) 165.
 26. X. Zhang, K. Xiao, C. Dong, J. Wu, X. Li and Y. Huang, *Eng. Fail. Anal.*, 18 (2011) 1981.
 27. E. Bidlas and R. J. W. Lambert, *Int. J. Food Microbiol.*, 124 (2008) 98.
 28. P. B. Raja, M. Fadaeinasab, A. K. Qureshi, A. A. Rahim, H. Osman, M. Litaudon and K. Awang, *Ind. Eng. Chem. Res.*, 52 (2013) 10582.
 29. J. Ning, Y. Zheng, D. Young, B. Brown and S. Nešić, *NACE Int.*, 70 (2014) 375.
 30. A. W. Decho, *Cont. Shelf Res.*, 20 (2000) 1257.
 31. H. C. Flemming, J. Wingender, U. Szewzyk, P. Steinberg, S. A. Rice and S. Kjelleberg, *Nat. Rev. Microbiol.*, 14 (2016) 563.
 32. D. Xu, Y. Li, F. Song and T. Gu, *Corros. Sci.*, 77 (2013) 385.